Manuscript prepared for Nonlin. Processes Geophys.
with version 5.0 of the LaTeX class copernicus.cls.
Date: 22 August 2014

Incidence and reflection of internal waves and wave-induced currents at a jump in buoyancy frequency

J. P. McHugh

University of New Hampshire, Durham, NH, USA

Correspondence to: J. P. McHugh
(john.mchugh@unh.edu)

Abstract. Weakly nonlinear internal gravity waves are treated in a two-layer fluid with a set of nonlinear Schrodinger equations. The layers have a sharp interface with a jump in buoyancy frequency approximately modelling the tropopause. The waves are periodic in the horizontal but modulated in the vertical and Boussinesq flow is assumed. The equation governing the incident wave packet is directly coupled to the equation for the reflected packet, while the equation governing transmitted waves is only coupled at the interface. Solutions are obtained numerically. The results indicate that the waves create a mean flow that is strong near and underneath the interface, and discontinuous at the interface. Furthermore, the mean flow has an oscillatory component that can contaminate the wave envelope, and has a vertical wavelength that decreases as the wave packet interacts with the interface.

1 Introduction

Earth's tropopause often has a vertical structure with a very sudden change in the lapse rate with increasing altitude, and a corresponding sudden increase in the buoyancy frequency N. This sudden increase in N can restrict upwardly propagating internal waves, as has been known for some time (Scorer, 1949). Observations of flow in the vicinity of the tropopause has also shown unusual dynamic behavior including high turbulence levels (Partl, 1962; Worthington, 1998; Wolff and Sharman, 2008; McHugh et al., 2008b) and large wave amplitudes (McHugh et al., 2008a; Smith et al., 2008). Turbulence and waves at these altitudes are important aspects of weather and climate, and serious hazards to aircraft.

McHugh (2008, 2009) considered horizontally periodic internal waves interacting with an idealized model of the tropopause. The waves in McHugh (2009) were uniform while the waves in McHugh (2008) were confined to a vertical packet and treated with numerical simulations. The results indicate that while nonlinear effects are stronger near the interface even with uniform waves, a modulated amplitude results in a localized jet-like mean flow near the interface that can be strong enough to form a critical layer, with important consequences for later waves.

Recently Grimshaw and McHugh (2013) treated weakly nonlinear two-layer horizontally periodic waves for both unsteady and steady flow. They show expressions for the wave-induced mean flow in both layers and show that this mean flow will be discontinuous at the interface, even when the waves have evolved into a steady flow. The same two-layer flow is treated here, now including the temporal evolution.

A related configuration is a layer with constant N (no interface), treated theoretically by Grimshaw (1975), Shrira (1981), Voronovich (1982), Sutherland (2006) and Tabaei and Akylas (2007). Grimshaw (1975) considered waves with a background shear flow using the wave action equation. Shrira (1981) treated weakly nonlinear waves in three dimensions assuming the modulation is the same in all directions. He derives the nonlinear Schrodinger equation that governs the wave packet evolution. Voronovich (1982) also treats weakly nonlinear waves but restricts attention to the special case with the modulation along a fixed direction. The weakly nonlinear waves in Sutherland (2006) are horizontally periodic with the modulation only in the vertical. Tabaei and Akylas (2007) treat weakly nonlinear and finite amplitude theory with several different configurations for the modulation. Associated numerical simulations with constant N were performed by Sutherland (2001) in two dimensions.

Packets of internal waves that propagate at a steep angle to the horizontal will experience a modulational instability, as discussed by Sutherland (2001). Wave packets experiencing this instability will focus wave energy. Waves propagating at

a shallow angle will defocus. For the waves treated here, this modulational instability may be important, depending on the wavenumbers and on the distance from the wave source to the interface. However for intermediate propagation angles, the modulational instability is too slow, and the waves interact with the interface before experiencing any significant effects.

The incident waves treated here are partially reflected at the interface, resulting in incident, reflected, and transmitted wave packets that are governed by coupled nonlinear Schrodinger (NLS) equations. Similar coupled NLS equations have been treated previously by Knobloch and Gibbon (1991) and Griffiths et al. (2006) starting with model equations such as the Klein-Gordon equation and groups of arbitrarily defined incident waves. The amplitude equations are similar to the equations given below.

The stability of plane monochromatic internal waves propagating at an angle to the horizontal were treated by Shrira (1981) and Tabaei and Akylas (2007), who showed that nonlinearity can lead to instability. Indeed Tabaei and Akylas (2007) show that the incident waves treated here are unstable for shallow angles. However the growth rate of the instability is second-order in the nonlinearity parameter, and hence the waves treated here will interact with the interface before this instability has time to grow significantly.

The reflection of nonlinear internal waves by a sloping bottom has been treated by several authors, for example Thorpe (1987) treats uniform wave trains and Tabaei et al. (2005) treat wave beams. The results show that the first few higher harmonics reflect at different angles than the primary harmonic while higher harmonics are evanescent, similar to waves reflecting from the interface treated in McHugh (2009). The mean flow in Thorpe (1987) has an oscillatory component parallel to the slope with wavenumber equal to the difference between incident and reflected wavenumbers, and this is also found here. The mean flow in Tabaei et al. (2005) is more complex as they considered wave beams, and they do not report an oscillatory component, however it is likely present in their calculations. Thorpe (1987) and Tabaei et al. (2005) do not include a modulation in the wave amplitude and their results do not have the associated mean flow. The mean flow that is present in Tabaei et al. (2005) is confined to the region where incident and reflected waves overlap. This same feature is true here only for the oscillatory part of the mean flow. Results for a rigid horizontal lid are given here at the end for comparison and show that the interface and the rigid lid have similar behavior. The rigid boundary creates a stronger mean flow due to the stronger reflected waves.

The results given below show that the incident and reflected waves combine for a short period to create a strong localized mean flow under the interface that is discontinuous at the interface, as in Grimshaw and McHugh (2013). Furthermore there is an oscillatory component of the mean flow with a vertical wavenumber that increases as the wave packet interacts with the interface. Section 2 provides the basic equations and interfacial boundary conditions. Section 3 chooses the wave modes to be included. Section 4 discusses the important mean flow, and then section 5 determines the amplitude equations. Results are discussed in section 6, followed by conclusions.

2 Basic equations

The flow is treated as incompressible and inviscid, and attention is restricted to two-dimensions. The stratification is due to the presence of a non-diffusing quantity, and the flow is assumed to be Boussinesq. The flow is then governed by

$$\frac{Du}{Dt} = -\frac{1}{\rho_0}\frac{\partial p}{\partial x}, \tag{1}$$

$$\frac{Dw}{Dt} = -\frac{1}{\rho_0}\frac{\partial p}{\partial z} - b, \tag{2}$$

$$\frac{\partial u}{\partial x} + \frac{\partial w}{\partial z} = 0, \tag{3}$$

$$\frac{Db}{Dt} - N^2 w = 0, \tag{4}$$

where

$$\frac{D}{Dt} = \frac{\partial}{\partial t} + u\frac{\partial}{\partial x} + w\frac{\partial}{\partial z},$$

the velocity is (u, w), the dynamic pressure is p, ρ_0 is an average (constant) density, b is the buoyancy, defined by

$$b = \frac{g(\rho - \tilde{\rho})}{\rho_0}, \tag{5}$$

$\tilde{\rho}$ is the background density, and N is the buoyancy frequency, defined by

$$N^2 = -\frac{g\tilde{\rho}_z}{\rho_0}. \tag{6}$$

The base state must satisfy the equation of static equilibrium,

$$\frac{\partial \tilde{p}}{\partial z} = -\tilde{\rho}g, \tag{7}$$

where $\tilde{p}$ is the background pressure. The lower and upper layers have buoyancy frequency N_1 and N_2, respectively.

The kinematic condition on the interface between the layers is

$$\eta_t + u\eta_x = w, \tag{8}$$

which holds on the interface $z = \eta$, where η is the vertical displacement of the interface. Expand in a Taylor series in the same manner usually used for free surface flow:

$$\eta_t + \left[u + u_z\eta + \frac{1}{2}u_{zz}\eta^2 + \cdots\right]\eta_x = \left[w + w_z\eta + \frac{1}{2}w_{zz}\eta^2 + \cdots\right], \tag{9}$$

now on $z = 0$.

The dynamic condition is continuity of total pressure p_T across the interface. The total pressure is segmented into two parts:

$$p_T = \tilde{p} + p. \tag{10}$$

As the pressure difference along the interface is zero, the directional derivative of the pressure difference along this interface is also zero. This directional derivative may be written as

$$\frac{\partial}{\partial x} + \eta_x \frac{\partial}{\partial z}, \tag{11}$$

which results in

$$\left[\Big(\frac{\partial}{\partial x} + \eta_x \frac{\partial}{\partial z} \Big) p + \eta_x \tilde{p}_z \right]_-^+ = 0 \tag{12}$$

on $z = \eta$. The equations of motion may now be used to eliminate the derivatives of the dynamic pressure, giving

$$\left[\Big(u_t + (uu)_x + (wu)_z \Big) + \eta_x \Big(w_t + (uw)_x + (ww)_z + b \Big) + \eta_x \frac{1}{\rho_0} \tilde{p}_z \right]_-^+ = 0 \tag{13}$$

on $z = \eta$. A Taylor series is used as before, leading to

$$\Big(1 + \eta \frac{\partial}{\partial z} + \cdots \Big) \left[\Big(u_t + (uu)_x + (wu)_z \Big) + \eta_x \Big(w_t + (uw)_x + (ww)_z + b \Big) \right]_-^+ - \eta_x \left[\eta N^2 + \frac{\eta^2}{2!} \frac{d}{dz} \Big(N^2 \Big) + \frac{\eta^3}{3!} \frac{d^2}{dz^2} \Big(N^2 \Big) + \cdots \right]_-^+ = 0 \tag{14}$$

on $z = 0$.

3 A vertically modulated wavetrain

The waves are horizontally periodic but modulated vertically. Define the following variables:

$$\begin{aligned} \xi &= x - c_p t, \\ \zeta &= \epsilon z, \\ \tau &= \epsilon t, \end{aligned} \tag{15}$$

where ϵ is small and measures the vertical packet length, and c_p is the horizontal phase speed.

The linear solution for a wave with upward group velocity is

$$w = \alpha I(\tau, \zeta) e^{i(k\xi - n_1 z)} + \text{cc}, \tag{16}$$

where k, n_1 are the horizontal and vertical wavenumbers, respectively. All wavenumbers are assumed positive. The dispersion relation is

$$c_p^2 = \frac{N_1^2}{k^2 + n_1^2}. \tag{17}$$

Here α is small and measures the strength of the vertical velocity, and cc means complex conjugate.

When an interface is included, the solution in the lower layer requires the addition of reflected waves:

$$\alpha R(\tau, \zeta) e^{i(k\xi + n_1 z)} + \text{cc}. \tag{18}$$

Higher harmonics are expected in a Boussinesq fluid with constant N (no interface) only as a result of the modulation, and these harmonics can be made weaker by choosing a slower modulation. The higher harmonics are $\bigcirc(\epsilon\alpha^2)$ and need not be included.

Further higher harmonics are generated by nonlinear effects at the interface, as shown previously by McHugh (2009). The modulation of the wavetrain does not exert the dominant influence on these interfacial harmonics, and in fact they occur even when the wave amplitude is constant (no wave packet). Hence these interfacial harmonics cannot be weakened by a slow modulation of the wave packet. However the vertical wavenumber of the interfacial harmonics is not commensurate with the primary harmonic. Hence these interface harmonics do not contribute to the evolution of the primary waves and also need not be included.

Combining all leading order contributions results in

$$w = \alpha I e^{i(k\xi - n_1 z)} + \alpha R e^{i(k\xi + n_1 z)} + \text{cc}, \; z < 0. \tag{19}$$

The corresponding solution for the upper layer is

$$w = \alpha T(\tau, \zeta) e^{i(k\xi - n_2 z)} + \text{cc}, \; z > 0. \tag{20}$$

The vertical wavenumber in the upper layer is n_2, determined to first-order by choosing the same k and frequency σ for the two layers:

$$\sigma = \frac{kN_1}{\sqrt{k^2 + n_1^2}} = \frac{kN_2}{\sqrt{k^2 + n_2^2}}. \tag{21}$$

The linear interfacial conditions result in a relationship between the amplitudes of the incident, reflected, and transmitted wave packets at the interface:

$$R = \mathcal{R} I, \tag{22}$$

$$T = \mathcal{T} I, \tag{23}$$

on $z = 0$, where

$$\mathcal{R} = \frac{n_1 - n_2}{n_1 + n_2}, \tag{24}$$

$$\mathcal{T} = \frac{2n_1}{n_1 + n_2}, \tag{25}$$

are the reflection and transmission coefficients, respectively.

4 The mean flow

Separate all dynamic fields into a ξ-averaged mean and a fluctuating part:

$$(u, w, p, b) = (\bar{u} + \alpha\hat{u},\ \bar{w} + \alpha\hat{w},\ \bar{p} + \alpha\hat{p},\ \bar{b} + \alpha\hat{b}), \tag{26}$$

where the bar indicates mean and the hat indicates the fluctuating part, composed of all wave components. The ξ-average will also be indicated with $< \cdot >$. Only the horizontal mean flow $\bar{u}$ is needed for the final amplitude equations.

A discussion of the general equations governing the wave-induced mean flow is given by Andrews and McIntyre (1978a,b) and Grimshaw (1979). In some cases an explicit expression for the mean may be found, as in Dosser and Sutherland (2011). Following Sutherland (2006), Grimshaw and McHugh (2013) found that for the present configuration and accurate to second-order in α,

$$\bar{u} = \frac{N^2}{c_p} < \chi^2 >,$$

$$\bar{w} = 0,$$

where χ is the vertical displacement. While the averaging in Grimshaw and McHugh (2013) is a x-average and therefore somewhat different, it is readily shown that the above expression is valid here with the ξ-average. The equation governing the evolution of χ is

$$\frac{D\chi}{Dt} = w,$$

however the linear version $-c_p\chi_\xi \approx w$ is adequate, and allows evaluation of $\bar{u}$ using (19) and (20). Finally, the mean flow in the lower layer is

$$\bar{u} = \bar{u}_m + \Big(\bar{u}_i e^{i2n_1 z} + \bar{u}_i^* e^{-i2n_1 z}\Big),\ z < 0, \tag{27}$$

where

$$\bar{u}_m = \frac{2}{c_p}\frac{N_1^2}{\sigma^2}\Big(II^* + RR^*\Big), \tag{28}$$

$$\bar{u}_i = \frac{2}{c_p}\frac{N_1^2}{\sigma^2} I^* R. \tag{29}$$

There are two parts to this mean flow. One part is $\bar{u}_m$, which is identical to the mean flow that would be obtained if the incident and reflected wave packets were acting individually, and the mean flows are merely added. The second part is the term containing $\bar{u}_i$, which is caused by the interference between the incident and reflected waves.

In the upper layer,

$$\bar{u} = \frac{2}{c_p}\frac{N_2^2}{\sigma^2} TT^*,\ z > 0. \tag{30}$$

5 The interaction equations

The leading order contributions to the primary harmonic in (1-4) will arise from linear terms and from interactions between the wave perturbations and the mean flow, as in Tabaei and Akylas (2007). Hence the leading-order primary-harmonic terms in (1-4) are

$$-c_p\hat{u}_\xi + \epsilon\hat{u}_\tau + \alpha^2\bar{u}\hat{u}_\xi + \alpha^2\bar{u}_z\hat{w} = -\frac{1}{\rho_0}\hat{p}_\xi, \tag{31}$$

$$-c_p\hat{w}_\xi + \epsilon\hat{w}_\tau + \alpha^2\bar{u}\hat{w}_\xi = -\frac{1}{\rho_0}\Big(\hat{p}_z + \epsilon\hat{p}_\zeta\Big) - \hat{b}, \tag{32}$$

$$\hat{u}_\xi + \hat{w}_z + \epsilon\hat{w}_\zeta = 0 \tag{33}$$

$$-c_p\hat{b}_\xi + \epsilon\hat{b}_\tau + \alpha^2\bar{u}\hat{b}_\xi - N^2\hat{w} = 0. \tag{34}$$

Formally eliminating $\hat{u}$, $\hat{b}$, and $\hat{p}$ from among these equations while dropping terms higher than quadratic in the small parameters results in

$$\Big(-c_p\frac{\partial}{\partial\xi} + \epsilon\frac{\partial}{\partial\tau}\Big)^2\Big[\Big(\frac{\partial}{\partial z} + \epsilon\frac{\partial}{\partial\zeta}\Big)^2 + \frac{\partial^2}{\partial\xi^2}\Big]w$$
$$-\alpha^2 c_p\frac{\partial^2}{\partial\xi^2}\Big[\bar{u}\Big(w_{\xi\xi} + w_{zz} + \frac{N^2}{c_p^2}w\Big) - \bar{u}_{zz}w\Big] = 0. \tag{35}$$

Equation (35) is a version of the Taylor-Goldstein equation for the present configuration. Using (19) and (20) in (35), again dropping higher order terms, and separating wave components results in three amplitude equations, one each for the incident, reflected, and transmitted wavetrains. For the incident waves the resulting equation is

$$\Big[D_tD_zD_tD_z - k^2\Big(D_t^2 + N_1^2\Big)\Big]I$$
$$-\alpha^2 2\sigma\Big[(k^2 + n_1^2)k\bar{u}_m I + (k^2 - n_1^2)k\bar{u}_i^* R\Big] = 0,$$
$$z < 0, \tag{36}$$

where

$$D_t = \epsilon\frac{\partial}{\partial\tau} - i\sigma, \tag{37}$$

$$D_z = \epsilon\frac{\partial}{\partial\zeta} - in_1. \tag{38}$$

Using the expressions for the mean flow, (27) and (30), and rearranging gives the final amplitude equation for the incident waves:

$$I_\tau + c_g I_\zeta - i\epsilon\frac{1}{2}c_g' I_{\zeta\zeta}$$
$$+ i\frac{\alpha^2}{\epsilon}\frac{2}{\sigma}\Big[\Big(k^2 + n_1^2\Big)\Big(|I|^2 + |R|^2\Big) + \Big(k^2 - n_1^2\Big)|R|^2\Big]I = 0,$$
$$z < 0, \tag{39}$$

where c_g is the vertical group velocity,

$$c_g = \sigma \frac{n_1}{k^2 + n_1^2},\ z < 0, \tag{40}$$

and c_g' is a derivative of the group velocity:

$$c_g' = \frac{\partial c_g}{\partial n_1} = \sigma \frac{k^2 - 2n_1^2}{(k^2 + n_1^2)^2},\ z < 0. \tag{41}$$

A similar development for the reflected and transmitted waves leads to

$$R_\tau - c_g R_\zeta - i\epsilon \frac{1}{2} c_g' R_{\zeta\zeta} + i\frac{\alpha^2}{\epsilon}\frac{2}{\sigma}\left[\left(k^2 + n_1^2\right)\left(|I|^2 + |R|^2\right) + \left(k^2 - n_1^2\right)|I|^2\right]R = 0, \quad z < 0, \tag{42}$$

$$T_\tau + c_g T_\zeta - i\epsilon \frac{1}{2} c_g' T_{\zeta\zeta} + i\frac{\alpha^2}{\epsilon}\frac{2}{\sigma}\left(k^2 + n_2^2\right)|T|^2 T = 0, \quad z > 0, \tag{43}$$

where

$$c_g = \sigma \frac{n_2}{k^2 + n_2^2},\ z > 0, \tag{44}$$

and

$$c_g' = \frac{\partial c_g}{\partial n_2} = \sigma \frac{k^2 - 2n_2^2}{(k^2 + n_2^2)^2},\ z > 0. \tag{45}$$

The interfacial conditions must be treated in the same manner. Keeping only quadratic terms,

$$\eta_t + (u\eta)_x = w, \tag{46}$$

$$\Big[u_t + (uu)_x + (uw)_z + \eta_x w_t + \eta u_{zt} + \eta_x b - N^2 \eta \eta_x\Big]_-^+ = 0, \tag{47}$$

on $z = 0$. Using (15), these are

$$-c_p \eta_\xi + \epsilon \eta_\tau + (u\eta)_\xi = w, \tag{48}$$

$$\Big[-c_p u_\xi + \epsilon u_\tau + (uu)_\xi + (uw)_z + \epsilon(uw)_\zeta - c_p \eta_\xi w_\xi + \epsilon \eta_\xi w_\tau - c_p \eta u_{z\xi} + \epsilon \eta u_{z\tau} - \epsilon c_p \eta u_{\zeta\xi} + \eta_\xi b - N^2 \eta \eta_\xi\Big]_-^+ = 0, \tag{49}$$

on $z = 0$, where higher-order terms have again been deleted. Using (26) and keeping only terms that contribute to the first harmonic gives

$$-c_p \hat{\eta}_\xi + \epsilon \hat{\eta}_\tau + \alpha^2 \bar{u} \hat{\eta}_\xi = \hat{w}, \tag{50}$$

$$\Big[-c_p \hat{u}_\xi + \epsilon \hat{u}_\tau + \alpha^2 \bar{u} \hat{u}_\xi\Big]_-^+ = 0, \tag{51}$$

on $z = 0$, after some simplification. Insert (19) and (20) along with associated expressions for the horizontal component of velocity into (50) and (51) and simplify to achieve a relationship between the reflected and transmitted wave amplitudes R, T and the incident wave amplitude I at the interface:

$$R + \epsilon \frac{i}{\sigma} R_\tau = \left[\frac{n_1 - n_2}{n_1 + n_2}\right]\left[I + \epsilon \frac{i}{\sigma} I_\tau\right] + \bigcirc(\alpha^2), \tag{52}$$

$$T + \epsilon \frac{i}{\sigma} T_\tau = \left[\frac{2n_1}{n_1 + n_2}\right]\left[I + \epsilon \frac{i}{\sigma} I_\tau\right] + \bigcirc(\alpha^2) \tag{53}$$

on $z = 0$. Hence nonlinear effects in the interfacial conditions are $\bigcirc(\alpha^2)$, which is two orders different from the leading order term in (52) and (53), and therefore higher order (as in (39), where quadratic terms are deleted). Hence the nonlinear effects in the interfacial conditions may be neglected with the present theory. The remaining terms in the interfacial conditions are balanced with the linear conditions,

$$R = \mathcal{R} I, \tag{54}$$

$$T = \mathcal{T} I, \tag{55}$$

on $z = 0$. Note that these conditions imply continuity of velocity of the wave components. Importantly the *total* velocity is not necessarily equal at the interface as the mean flow may not be continuous.

6 Results

The amplitude equations (39), (42), and (43) are solved here numerically. Spatial derivatives are evaluated with second-order central differences. Temporal integration is achieved with the fourth-order Adams-Bashforth method, resulting in explicit algebraic equations (see Ames (1977) for a general discussion). The boundary point at the end of the domain is treated with the second-order upwind scheme. This one-sided method allows waves to exit the region without reflections (the reflected waves have already been treated in the derivation of the amplitude equations). Single-layer cases discussed below employ a total resolution of 1600 gridpoints while two-layer cases use 800 gridpoints in each layer, which was found to be adequate for all parameter values. The depth of each layer for two-layer cases was set to $4/3$ of the packet length, which also sets the grid spacing. Several cases were treated with double this resolution to confirm convergence. The time step was set to avoid numerical instability, generally being in the range $0.0001 < \Delta t < 0.001$.

All variables are rescaled with the horizontal wavenumber k and the buoyancy frequency in the lower layer N_1. The buoyancy frequency ratio for two-layer cases is chosen to have the value $N_2/N_1 = 2$, matching approximately Earth's

tropopause. The results then depend on three parameters: ϵ, α, and n_1/k. The parameter ϵ is set to be equal to the inverse of the packet length, and is chosen to have the value $\epsilon = 0.025$. Different values of ϵ generally showed the same results as discussed below. The value of α is set to $\alpha = 0.1$. Larger values of α means stronger nonlinear effects, with consequences that depend on the value of n_1/k.

A wave envelope is created at the bottom boundary by imposing the value of the real part of I to be the raised cosine function:

$$I = \frac{1}{2}\left[1 - \cos\frac{\tau}{\epsilon c_g}\right], \tag{56}$$

$\tau \in [0, \epsilon c_g]$, where ϵc_g is equivalent to the wave period times the number of waves in the wave packet. Other wave packet shapes, such as a Gaussian shape, have been considered and produce the same general results.

The behavior of the waves with increasing n_1/k is complicated, and depends partly on the value of the reflection and transmission coefficients $\mathcal{R}$, $\mathcal{T}$ given by (24) and (25), see figure 1. For very small values of n_1/k, $\mathcal{R}$ approaches unity while $\mathcal{T}$ approaches zero, indicating that the waves are nearly perfectly reflected. As n_1/k increases, $\mathcal{R}$ approaches the value $1/3$ while $\mathcal{T}$ approaches $2/3$. Hence for large values of n_1/k, the reflection and transmission coefficients are approximately constant. Perfect transmission never occurs for any value of n_1/k.

The behavior with increasing n_1/k also depends greatly on the strength of the mean flow. The results given below will show that the mean flow given in (27) and (30) increases strongly with n_1/k, as measured approximately by the factor $\frac{N_1^2}{c_p \sigma^2}$. This increase is primarily due to the direction of the group velocity becoming more horizontal as n_1/k increases. Define U to be this factor, which after rescaling becomes

$$U = 2\Big(\frac{k^2 + n_1^2}{k^2}\Big)^{3/2}. \tag{57}$$

Profiles of the mean flow velocity appearing in the figures are normalized by U.

The coefficient of the nonlinear term and the dispersion term in the amplitude equation governing the incident waves (39) are plotted in figure 2. The coefficient value for the nonlinear term can be seen to increase strongly with n_1/k, as a direct result of the mean flow dependence on n_1/k. Hence stronger nonlinear effects are expected as n_1/k increases.

The dispersion coefficient is negative for small values of n_1/k, and changes sign at $n_1/k = 1/\sqrt{2}$. As discussed by Sutherland (2001), the waves experience a modulational instability in the region where this coefficient is negative. As a result of this instability, a wave packet will initially become more focused and grow in amplitude. This dispersion coefficient is positive for $n_1/k > 1/\sqrt{2}$ and reaches a maximum at $n_1/k = \sqrt{2}$. When the coefficient is positive, the wave packet defocuses.

Some insight is revealed by separating the wave amplitude into a magnitude and phase,

$$I = |I| e^{i\phi},$$

where ϕ is the phase of the incident waves. Using this in (39) and separating real and imaginary parts results in

$$|I|_\tau + c_g |I|_\zeta + \epsilon \frac{1}{2} c_g' \Big[|I| \phi_{\zeta\zeta} + 2 |I|_\zeta \phi_\zeta \Big] = 0, \tag{58}$$

$$\phi_\tau + c_g \phi_\zeta + \epsilon \frac{1}{2} c_g' \Big[\frac{|I|_{\zeta\zeta}}{|I|} - \phi_\zeta^2 \Big] + \frac{\alpha^2}{\epsilon} \frac{1}{2} \Big[(k^2 + n_1^2)(|I|^2 + |R|^2) + (k^2 - n_1^2)|I|^2 \Big] = 0. \tag{59}$$

Similar equations can be obtained for the other wave packets. Equation (58) governs the evolution of the magnitude of the the incident wave $|I|$. The influence of the reflected wave R does not directly appear in (58). Hence when incident and reflected waves overlap, the reflected wave only affects the incident wave packet shape as a result of the evolution of ϕ in the dispersion term. For cases where the dispersive effect is zero or negligible, then (58) becomes

$$|I|_\tau + c_g |I|_\zeta = 0, \tag{60}$$

indicating that the wave packet propagates with the group velocity c_g but without any evolution in the packet shape, and unaffected by the reflected wave even when overlapping.

Multiply (58) by $|I|$ and rearrange to obtain

$$\Big(\frac{\partial}{\partial \tau} + c_g \frac{\partial}{\partial \zeta} \Big) |I|^2 + \epsilon c_g' \frac{\partial}{\partial \zeta} \Big(|I|^2 \phi_\zeta \Big) = 0.$$

For time periods before the incident wave packet reaches the interface, this may be integrated to produce

$$\frac{\partial}{\partial \tau} \int |I|^2 \, d\zeta = 0, \tag{61}$$

where boundary terms are zero since $|I|$ is zero outside the wave packet. Equation (61) shows that the spatial integral of $|I|^2$ is conserved in a layer of constant N, despite the influence of dispersion and nonlinearity. Once the incident wave packet reaches the interface, the incident wave packet begins to decrease in area as the reflected and transmitted waves are created. The combination of (58), which shows that $|I|$ is not influenced by nonlinear effects, and (61), which shows that the area of the wave packet is limited, suggest that the incident wave packet shape will decrease monotonically during this time.

Equation (59) governs the incident wave phase, and does explicitly contain R. The effect of the dispersion term is complicated and will be determined with numerical results. However the nonlinear term in (59) is positive, and in the absence

of dispersion,

$$\Big(\frac{\partial}{\partial\tau}+c_g\frac{\partial}{\partial\zeta}\Big)\phi<0.$$

Hence the nonlinear effect causes the phase to decrease, resulting in an increase in the oscillations in the phase.

For the numerical results, first consider constant N throughout and let $n_1/k=1/\sqrt{2}$. This special value of n_1/k has a zero value for the coefficient of the dispersion term. Figure 3 shows vertical profiles of wave amplitude and mean flow at three times for this case. Note that a time value of zero here corresponds to the wave packet centered at the origin, which is also the mean position of the interface in two-layer cases. Each time value in figure 3 shows three panels, which contain (from left to right in each subfigure) a vertical profile of the wave magnitude, the wave phase, and the wave-induced mean flow. Comparing the left panel in figure 3a to that in figure 3b and 3c, it can be seen that the wave packet moves vertically without any significant change in shape, as predicted by (60). The phase ϕ under these same conditions obeys

$$\phi_\tau+c_g\phi_\zeta+\frac{\alpha^2}{\epsilon}(k^2+n_1^2)|I|^2=0. \tag{62}$$

Since $|I|$ is constant for this case when moving with the packet, the phase will decrease linearly as a result of nonlinearity, as can be seen in figure 3, where oscillations in phase develop as the packet ascends.

A corresponding two-layer case is shown in figure 4 using the same $n_1/k=1/\sqrt{2}$ value as the above one-layer case. The Brunt-Vaisala frequency ratio is $N_2/N_1=2$ and the interface is at the center of each panel ($z=0$) as indicated with a dashed line. The three time values are chosen to correspond to (a) before the wave packet has reached the interface, (b) as the packet is transiting the interface, and (c) after the packet has passed through the interface. The dashed profiles are the magnitude and phase for the downward moving wave packet (the reflected wave), and the solid profiles are the upward moving waves (incident and transmitted waves). Note that there is only a single profile for the mean flow in the lower layer (e.g. no dashed profile) as it is due to the combination of incident and reflected waves.

The packet in figure 4a has not interacted with the interface yet, and hence is identical to the constant N case in figure 3a. Figure 4b has all three wave packets present simultaneously. The mean flow at this stage shows the striking discontinuity at the interface. The reason for this discontinuity is that in the lower layer the mean flow is driven by both incident and reflected wave. Since they both have a horizontal component of group velocity that is positive, then the mean flow they generate is positive, despite having a vertical group velocity that has opposite sign. In contrast, the upper layer only has the transmitted wave driving a mean flow, and is therefore always weaker, even at the interface.

The mean flow in figure 4b also shows oscillations that are not present before the packet reaches the interface or in the single layer case. These oscillations are due to the interference mean given by (27) and (29). The interference mean only occurs *under* the mean position of the interface, and only when the incident wave and reflected wave are overlapping.

Without dispersion (c_g' is zero in the lower layer when $n_1/k=1/\sqrt{2}$), the magnitude of the incident waves $|I|$ for the two-layer case is governed by (60), however the phase now obeys

$$\phi_\tau+c_g\phi_\zeta+\frac{\alpha^2}{\epsilon}\frac{2}{\sigma}\Big[(k^2+n_1^2)(|I|^2+|R|^2)+(k^2-n_1^2)|I|^2=0. \tag{63}$$

Similarly for the reflected wave packet,

$$|R|_\tau+c_g|R|_\zeta=0, \tag{64}$$

$$\theta_\tau-c_g\theta_\zeta+\frac{\alpha^2}{\epsilon}\frac{2}{\sigma}\Big[(k^2+n_1^2)(|I|^2+|R|^2)+(k^2-n_1^2)|R|^2=0, \tag{65}$$

where θ is the phase of the reflected waves. Equation (64) shows that the magnitude of the reflected waves is not affected by lingering presence of the incident waves (and vice versa as discussed above). However (63) shows that the phase of the incident waves is connected to the magnitude of both incident and reflected waves, as is the phase of the reflected wave, see (65). Furthermore, since the nonlinear term in both (63) and (65) is always positive, then the phase for both incident and reflected waves decreases monotonically.

Figure 4c shows a later time, after the incident wave packet has been completely converted into reflected and transmitted wave packets. The wave-induced mean flow is now much reduced in strength as a result of the smaller amplitude of both transmitted and reflected waves, as compared to the incident wave in figure 4a. The reflected wave packet retains the original shape of the incident wave packet with no apparent change due to the nonlinear interaction at the interface. The coefficient of dispersion in the upper layer is not zero, and the wave packet shape can be seen to have evolved somewhat in figure 4c.

A close-up view of the wave amplitude as the wave packet is transiting the interface is shown in figure 5 for a sequence of time values, each profile shifted by a value of 1.5 for display. Note that the disturbance velocity in this model is continuous, even though it appears to be discontinuous in figure 5. Figure 6 shows corresponding profiles of the mean flow, which is indeed discontinuous at the interface during this period. The discontinuity is formed by the 'front' of the wave packet and would then be maintained until the 'back'

of the wave packet terminates the mean flow. Thus the discontinuous flow would remain if the waves evolved into a uniform field, rather than the finite packet treated here.

The coefficient of the dispersion term is negative when $n_1/k < 1/\sqrt{2}$. The evolution of the wave packet for such a case is shown in figure 7 for a single layer with constant N and $n_1/k = 0.4$. This same single-layer case was previously treated by Sutherland (2001, 2006), and Tabaei and Akylas (2007). Figure 7a shows that the wave amplitude and the associated mean flow are initially focusing energy toward the center of the wave packet. Figures 7b and 7c show that at later times the peak in wave amplitude has decreased and the wave packet has spread significantly. Even longer times would show the focusing effect reappearing. This behavior is due to the modulational instability as discussed by Sutherland (2001). Figure 8a provides filled contours of vertical velocity for the same time value as figure 7a, demonstrating the same general pattern as was found by Sutherland (2006). Figure 8b shows the pattern at a later time after the wave amplitude has reached it's peak and is decreasing.

The two layer case with $n_1/k = 0.4$ is shown in figure 9. Figure 9a is before the incident wave packet has interacted significantly with the interface, and again the results are the same as the constant N case, figure 7a. In Figure 9b the wave packet is straddling the interface. The mean flow (right panel) again shows the oscillations under the interface that is the interference part of the mean flow $\bar{u}_i$, although these oscillations are somewhat difficult to see due to the different scale on the abscissa. Also evident in figure 9b are matching oscillations in I (solid line for both magnitude and phase). These oscillations would not exist without dispersion, as I obeys (60) without dispersion. Note that these oscillations in I were not present with $n_1/k = 1/\sqrt{2}$ in figure 4b.

Figure 9c shows the results at a later time after the reflected and transmitted wave packets are mostly created. The magnitude of I (solid line, left panel) still shows significant oscillations, while the magnitude of R (dashed line, left panel) does not. The mean flow also has matching oscillations. The incident waves I can only move upwards here, hence these oscillations in I are part of the tail of the incident wave packet. Dispersion has caused the incident wave packet to spread, which continues to interact with the downward moving reflected wave packet. For this choice of parameters ($\epsilon = 0.025, \alpha = 0.1$), the incident wave amplitude I had reached it's maximum before interacting with the interface and is decreasing while the packet is spreading. This feature of the wave packet dynamics seems to enhance the interaction between the reflected waves and the tail of the incident packet.

Figures 10 and 11 again show a close-up view of the wave amplitudes and mean flow near the interface. Figure 10 shows clearly the formation of these smaller scale oscillations in I, and seems to suggest that they are moving downward. However they are not moving downward but becoming energized by the downward moving reflected wave R.

Figure 12 shows filled contours of vertical velocity, corresponding to the constant N case in figure 8b. The wave pattern under the interface in figure 12 (the interface is at the ordinate center) with incident and reflected waves overlapping is nearly that of a standing wave.

Figures 13 and 14 show results for a case when the coefficient of dispersion is positive, $n_1/k = 1$. Figure 13 is the single-layer case with constant N while figure 14 is the corresponding two-layer configuration with $N_2/N_1 = 2$. Figure 13 shows that as the wave packet ascends in a single layer, the packet shape tends to spread. The two-layer results in figure 14b show that the mean flow is again discontinuous as the wave packet interacts with the interface, and that the interference mean is again present. Oscillations in I appear and spread downward, as before. However the dispersion effect is dominant here and the transmitted and reflected wave packets are much reduced in strength as a result. The nonlinear aspects of the waves become very weak for this case.

The amplitude and phase are governed by (58) and (59). One of the nonlinear terms in (59) is directly attributed to the interference mean flow, and has the rescaled coefficient

$$1 - \frac{n_1^2}{k^2}. \tag{66}$$

If $n_1/k = 1$ then this coefficient is zero, and hence this nonlinear term does not contribute to the evolution of ϕ, making $n_1/k = 1$ a special case. The influence of the interference part of the mean flow is still felt but indirectly through the other nonlinear terms in (58) and (59).

Figures 15 and 16 again show a close-up view of a sequence of profiles of the wave magnitude and corresponding mean flow as the packet transits the interface. Figure 16 shows the development of the discontinuity in the mean flow as well as the appearance of the interference mean flow. Another feature evident in figure 16 is that the oscillations in the mean flow under the interface are decreasing in length as time increases. The form of (27) suggests that the oscillation length should be simply $2\pi/2n_1$, which it is when these oscillation first appear. However the nonlinear combination of I and R alters this length. The effect is present for previous cases but is not as prominent.

Figure17 shows results for the two-layer case with $n_1/k = \sqrt{2}$. This value of n_1/k corresponds to the maximum value of the dispersion coefficient in the amplitude equations for the lower layer. With such strong dispersion, the wave packet spreads considerably by the time the packet reaches the interface. The numerical results indicate that with such strong dispersion, increasing the value of α weakens the interference mean and the tendency for these oscillations in the mean flow to shorten.

The overall mean-flow strength near the interface is shown in figures 18-20 for three examples. Each of these figures show a time evolution of the maximum of the wave packet amplitude. In figure 18, $n_1/k = 1/\sqrt{2}$ and the dispersion is zero in the lower layer. For this case the maximum value of

the wave amplitude is constant until the waves interact with the interface. While the packet is near the interface, the mean flow is enhanced due to the combination of the incident and reflected waves, and also the interference mean. Figure 18 shows that the mean flow is enhanced by a factor of approximately 1.75 at the peak. Figure 19 has $n_1/k = 0.4$ and shows that the maximum value is nearly four times the value of the mean flow early in the simulation. Also evident here is the oscillation in the tail of the incident wave packet.

Figure 20 has $n_1/k = \sqrt{2}$ where the dispersion coefficient is positive and maximum. Here the wave packet is defocusing, resulting in a decrease in the maximum value as the wave packet ascends. The increase in mean at the interface is not strong enough to overcome this decrease, and hence the maximum value of mean flow is at the beginning of the simulation. Overall, figures 18-20 indicate that smaller values of n_1/k are more likely to have an enhanced jet-like mean flow under the interface.

Also in figures 18-20 is a dashed line showing the velocity difference at the interface, and a thick solid line showing the maximum of the interference mean. In figure 18 and 20, these two quantities are approximately the same. However the velocity difference is not caused by the interference mean, rather they are both caused by the overlapping of the incident and reflected wave packets, and hence have approximately the same strength. Note the velocity difference for $n_1/k = 0.4$ in figure 19 is substantially stronger than the interference mean in figure 18.

If the interface is replaced with a rigid lid, then the waves are completed reflected, but otherwise behave in the same manner as above. The interfacial boundary conditions are replaced with

$$w = 0 \tag{67}$$

on $z = 0$, resulting in

$$R = -I \tag{68}$$

on $z = 0$. The incident and reflected wave amplitudes are still governed by (39) and (42), while the mean flow is still determined with (27).

An example case with $n_1/k = 1/\sqrt{2}$ is shown in figure 21 with vertical profiles of wave magnitude and phase and the mean flow at three time steps, as before. Notice in figure 21 that the wave magnitude and mean flow when the packet is moving upward ($N_1\tau \approx -65$) have the same profile after bouncing off the rigid lid and is moving downward ($N_1\tau \approx +65$). The only difference other than the direction of propagation is the phase which is more oscillatory. The mean flow for $N_1\tau \approx 0$ is much stronger than the above case with an interface as a result of the much stronger reflected wave. The maximum of the mean flow is now approximately three times the mean flow of the incident wave packet, compared to a factor of 1.75 in the case with the interface. The interference mean flow is still clearly present with the rigid lid.

7 Conclusions

Atmospheric observations indicate that the tropopause altitude is more likely to experience turbulence and large amplitude waves than other altitudes. The abrupt change in the buoyancy frequency suggests that such observations are related to the dynamics of internal waves near the tropopause. Previous numerical simulations conclude that internal waves will create a wave-induced jet-like mean flow in the tropopause vicinity that is likely responsible for at least some of the observations. An idealized low-dimensional model of such waves is treated here. The model consists of three coupled nonlinear Schodinger equations.

Numerical solutions with with weak dispersion ($n_1/k = 1/\sqrt{2}$) show that the wave-induced mean flow is greatest near and under the interface, similar to previous full numerical simulations by McHugh (2008). Furthermore, this mean flow is discontinuous at the interface, and would be a region of strong shear in a viscous flow. The previous full numerical results did not allow the velocity to be discontinuous at the interface, and this could have impacted the final results in that study.

However, the results here also show that dispersion may dominate the motion, and can act to greatly enhance the jet-like flow or weaken it, depending on the value of n_1/k. With $n_1/k < 1/\sqrt{2}$, the jet-like mean flows are strengthened and they can happen at any altitude, not necessarily near the interface. With $n_1/k > 1/\sqrt{2}$, dispersion tends to smooth the localised effects near the interface.

The mean flow found here also has the oscillatory interference component. The results show that these mean-flow oscillations are transferred to the wave envelopes, and can get exaggerated in the tail of the incident wave packet when $n_1/k < 1/\sqrt{2}$. Furthermore, the vertical wavelength of the oscillation decreases during the period where incident and reflected waves overlap. These are nonlinear features of the waves that do not occur in linear theory. Note that this feature of the mean flow indicates that the waves create a structure that is wider horizontally than the incident waves, but shorter in the vertical. Hence there is a cascade of energy to 'flatter' structures.

The observations of McHugh et al. (2008a) showed layers at the tropopause region with large values of vertical velocity. The terrain was dominated by a single large peak (Mauna Kea), and thus these structures were likely caused by mountain waves. There are many similarities between those experimental results and the present model results, most notably, the mean flow oscillations in the model are similar to the layer structure in the experiments. However, differences are also significant, for example, the experiments show large *vertical* velocity whereas the model finds large *horizontal* velocity. A detailed comparison is difficult since the experiments treated mountain waves, a much more complex wave system. Hence it is tempting but premature to connect the mean flow

oscillations found here to the structures observed in McHugh et al. (2008a).

References

Ames, W. F.: Numerical methods for partial differential equations, Academic Press, 1977.

Andrews, D. G. and McIntyre, M. E.: An exact theory of nonlinear waves on a Lagangian-mean flow, J. Fluid Mech., 89, 609–646, 1978.

Andrews, D. G. and McIntyre, M. E.: On wave action and it's relatives, J. Fluid Mech., 89, 647–664, 1978.

Dosser, H. V. and Sutherland, B. R., Weakly nonlinear non-Boussinesq internal gravity wavepackets, Physica D, 240, 346–356. 2011.

Griffiths, S. D. and Grimshaw, R. H. J. and Khusnutdinova, K. R.: Modulational instability of two pairs of counter-propagating waves and energy exchange in a two-component system, Physica D, 214, 1–24, 2006.

Grimshaw, R. H. J.: Nonlinear internal gravity waves and their interaction with the mean wind, J. Atmos. Sci., 32, 1779–1793, 1975.

Grimshaw, R. H. J.: Mean flows induced by internal gravity wave packets propagating in a shear flow, J. Fluid Mech., 90, 161–178, 1979.

Grimshaw, R. and McHugh, J. P.: Steady and unsteady nonlinear internal waves incident on an interface, Q. J. Roy. Met. Soc., 139, 1990–1996, 2013.

Knobloch, E. and Gibbon, J. D.: Coupled NLS equations for counter propagating waves in systems with reflection symmetry, Phy. Let. A, 154, 353–356, 1991.

McHugh, J. P.: Mean flow generated by an internal wave packet impinging on the interface between two layers of fluid with continuous density, Theo. Comp. Fluid Dyn., 22, 107–123, 2008.

McHugh, J. P. and Dors, I. and Jumper, G. Y. and Roadcap, J. and Murphy, E. and Hahn, D.: Large variations in balloon ascent rate over Hawaii, J. Geo. Res., 113, 2008a.

McHugh, J. P. and Jumper, G. Y. and Chun, M.: Balloon thermosonde measurements over Mauna Kea, and comparison with seeing measurements, Pub. Astro. Soc. Pac., 120, 1318–1324, 2008b.

McHugh, J. P.: Internal waves at an interface between two layers of differing stability, J. Atmos. Sci., 66, 1845–1855, 2009.

Partl, W.: Clear air turbulence at the tropopause levels, Navigation, 9, 288–295, 1962.

Scorer, R. S.: Theory of waves in the lee of mountains, Q. J. Roy. Met. Soc., 75: 41–56, 1949.

Smith, R. B. and Woods, B. K. and Jensen, J. and Cooper, W. A. and Doyle, J. D. and Jiang, Q. and Grubisic, V.: Mountain waves entering the stratosphere, J. Atmos. Sci., 65, 2543–2562, 2008.

Shrira, V. I.: On the propagation of a three-dimensional packet of weakly non-linear internal gravity waves, Int. J. Non-linear Mech., 16, 129–138, 1981.

Sutherland, B. R.: Finite-amplitude internal wavepacket dispersion and breaking, J. Fluid Mech., 429, 343–380, 2001.

Sutherland, B. R.: Weakly nonlinear internal gravity wavepackets, J. Fluid Mech., 569, 249–258, 2006.

Tabaei, A. and Akylas, T. R. and Lamb, K. G.: Nonlinear effects in reflecting and colliding internal wave beams, J. Fluid Mech., 526, 217–243, 2005.

Tabaei, A. and Akylas, T. R.: Resonant long-short wave interactions in an unbounded rotating stratified fluid, Stud. Appl. Math., 119, 271–296, 2007.

Thorpe, S. A.: On the reflection of a train of finite-amplitude internal waves from a uniform slope, J. Fluid Mech., 178, 279–302, 1987.

Voronovich, A. G.: On the propagation of a packet of weakly nonlinear internal waves in a medium with constant Vaisala frequency, Izv. Atmos. Ocean Phy., 18, 247–250, 1982.

Wolff, J. K. and Sharman, R. D.: Climatology of upper-level turbulence over the contiguous United States, J. Appl. Meteor. Climatol., 47, 2198–2214, 2008.

Worthington, R. M.: Tropopausal turbulence caused by the breaking of mountain waves, J. Atmos. Sol.-Terr. Phy., 60, 1543–1547, 1998.

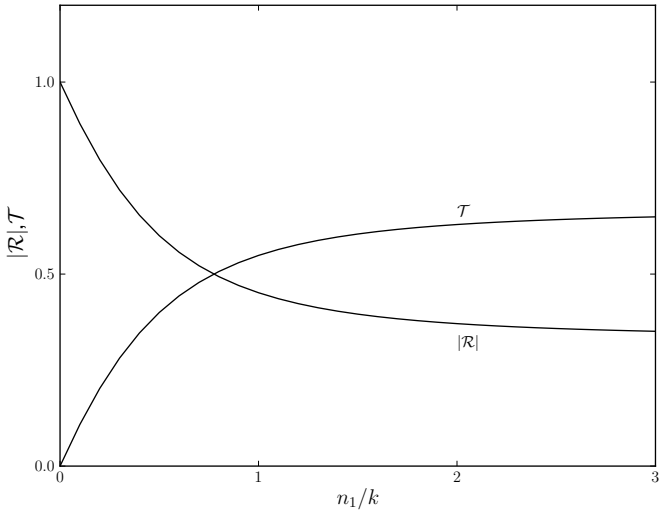

Fig. 1: Transmission coefficient $\mathcal{T}$ and absolute value of the reflection coefficient $|\mathcal{R}|$ as n_1/k increases.

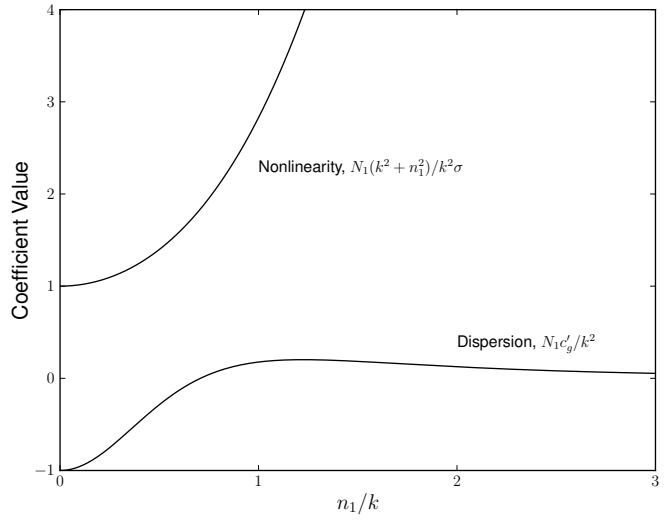

Fig. 2: Behavior of the coefficients of the dispersion and nonlinear terms in the amplitude equations as n_1/k increases.

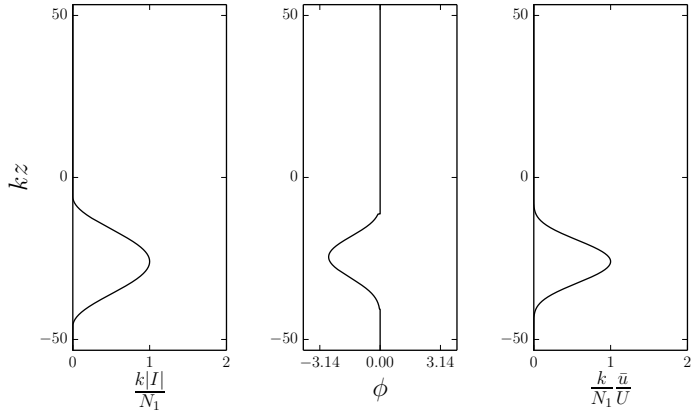

(a) $N_1\tau \approx -75$

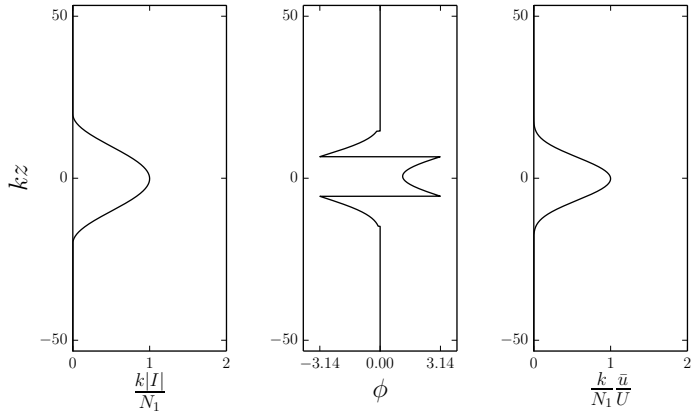

(b) $N_1\tau \approx 0$

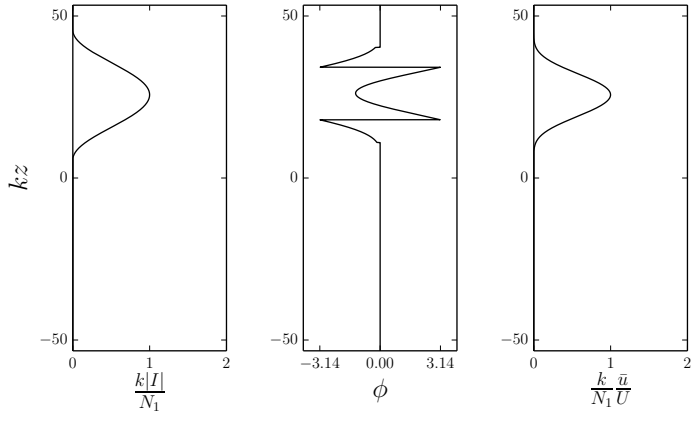

(c) $N_1\tau \approx +75$

Fig. 3: Vertical profiles of the wave magnitude (left panel), phase (center panel), and mean flow (right panel) at three times in a single layer of constant N with $n_1/k = 1/\sqrt{2}$, $\epsilon = 0.025$, and $\alpha = 0.1$.

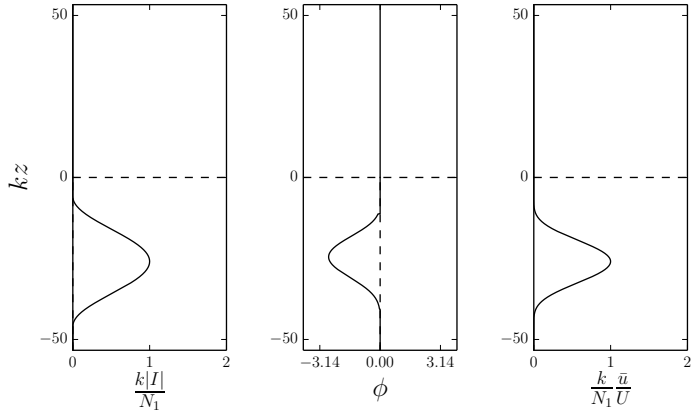

(a) $N_1\tau \approx -75$

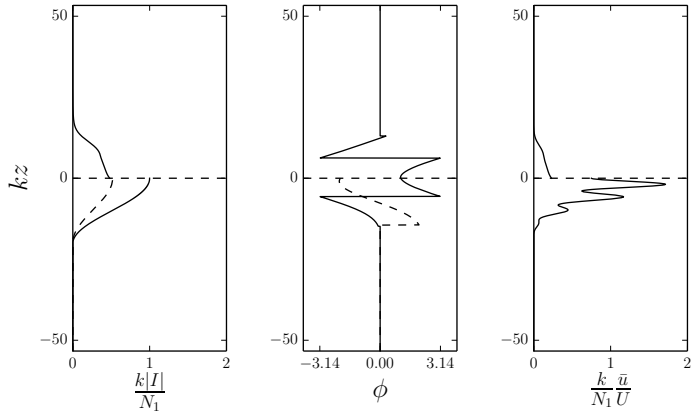

(b) $N_1\tau \approx 0$

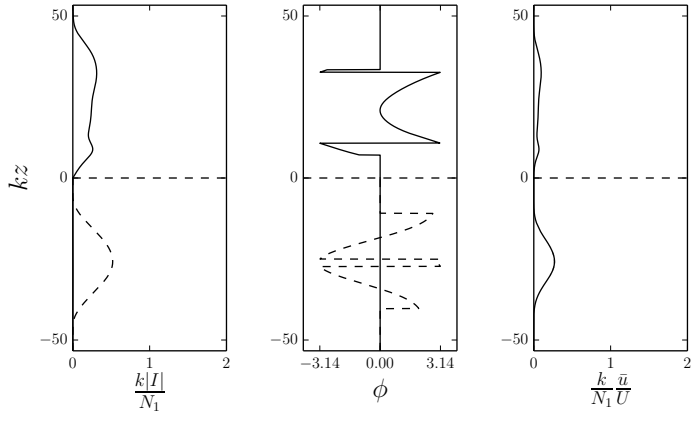

(c) $N_1\tau \approx +75$

Fig. 4: Vertical profiles of the wave magnitude (left panel), phase (center panel), and mean flow (right panel) at three times in two layers. The parameter values are $n_1/k = 1/\sqrt{2}$, $N_2/N_1 = 2$, $\epsilon = 0.025$, and $\alpha = 0.1$.

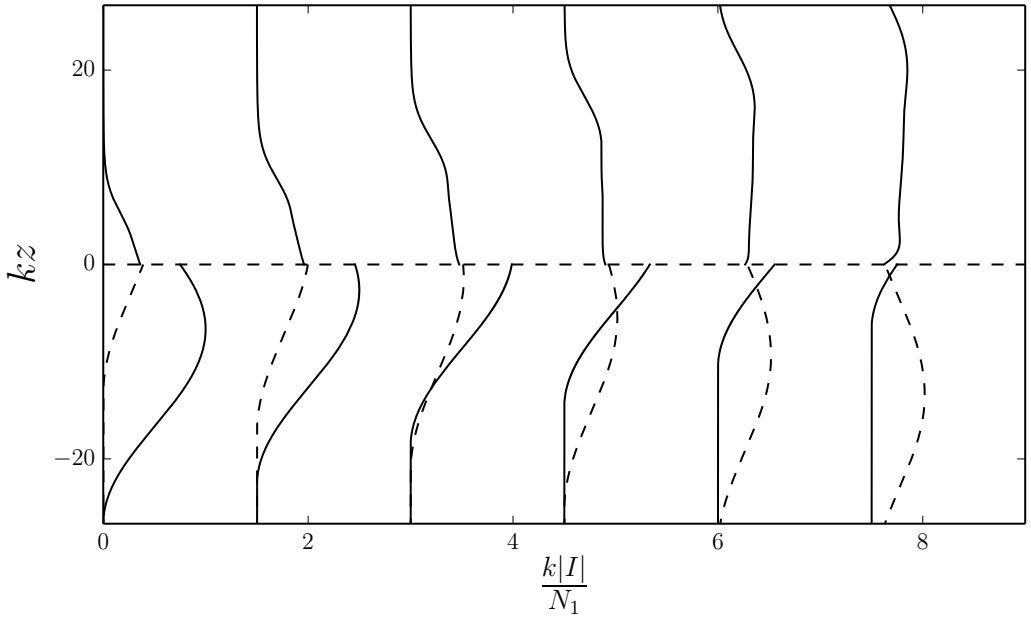

Fig. 5: Vertical profiles of the wave magnitude in two layers for a sequence of times. Each profile is shifted by a value of 1.5 for display. The parameter values are $n_1/k = 1/\sqrt{2}$, $N_2/N_1 = 2$, $\epsilon = 0.025$, and $\alpha = 0.1$.

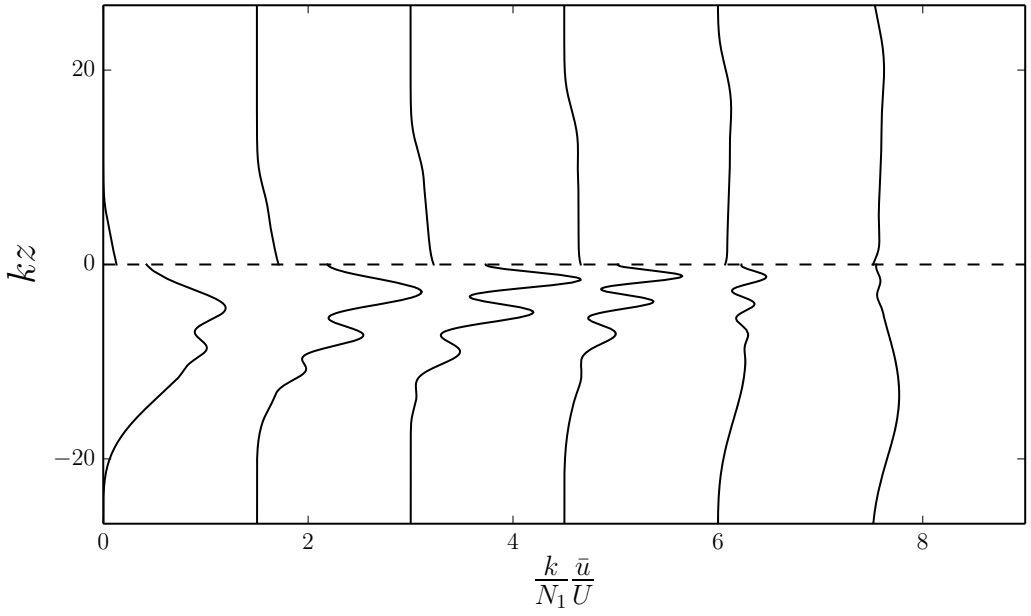

Fig. 6: Vertical profiles of the mean flow in two layers for a sequence of times. Each profile is shifted by a value of 1.5 for display. The parameter values are $n_1/k = 1/\sqrt{2}$, $N_2/N_1 = 2$, $\epsilon = 0.025$, and $\alpha = 0.1$.

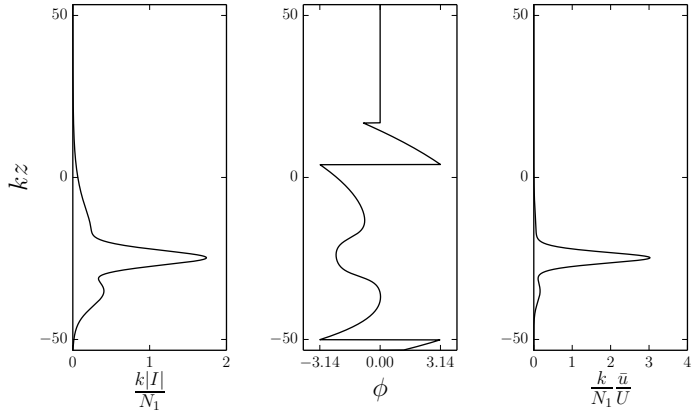

(a) $N_1\tau \approx -80$

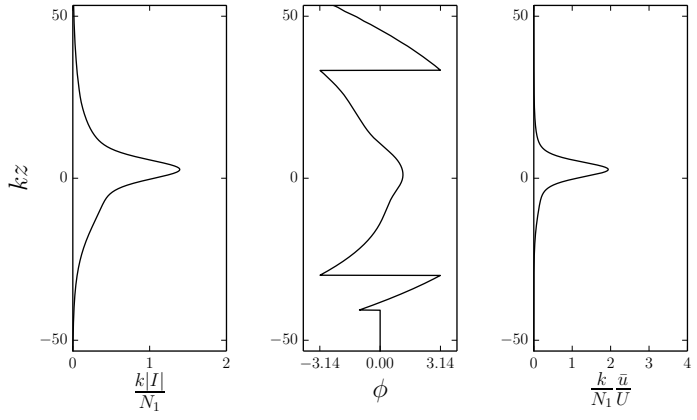

(b) $N_1\tau \approx 0$

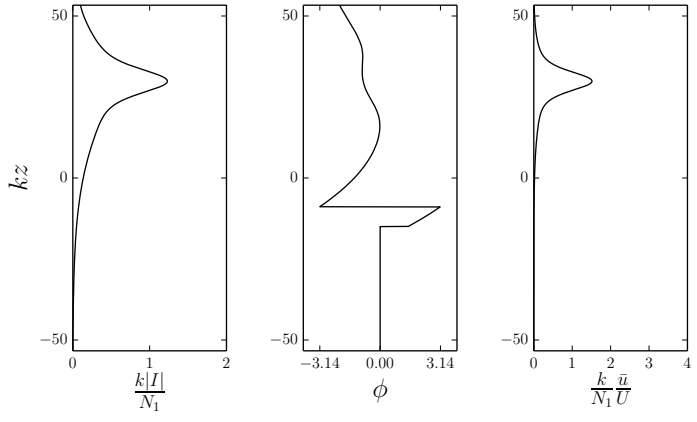

(c) $N_1\tau \approx +80$

Fig. 7: Vertical profiles of the wave magnitude (left panel), phase (center panel), and mean flow (right panel) at three times in a single layer of constant N with $n_1/k = 0.4$, $\epsilon = 0.025$, and $\alpha = 0.1$.

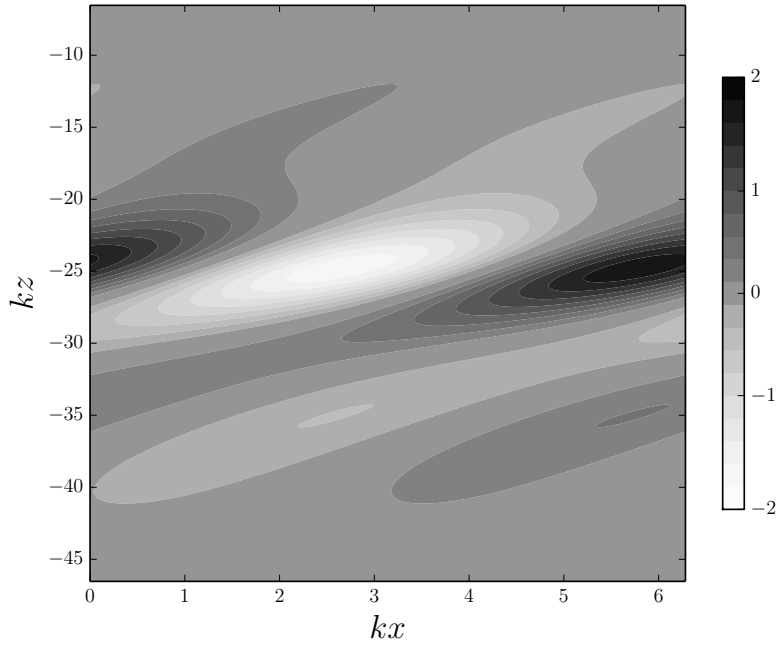

(a) $N_1\tau \approx -80$

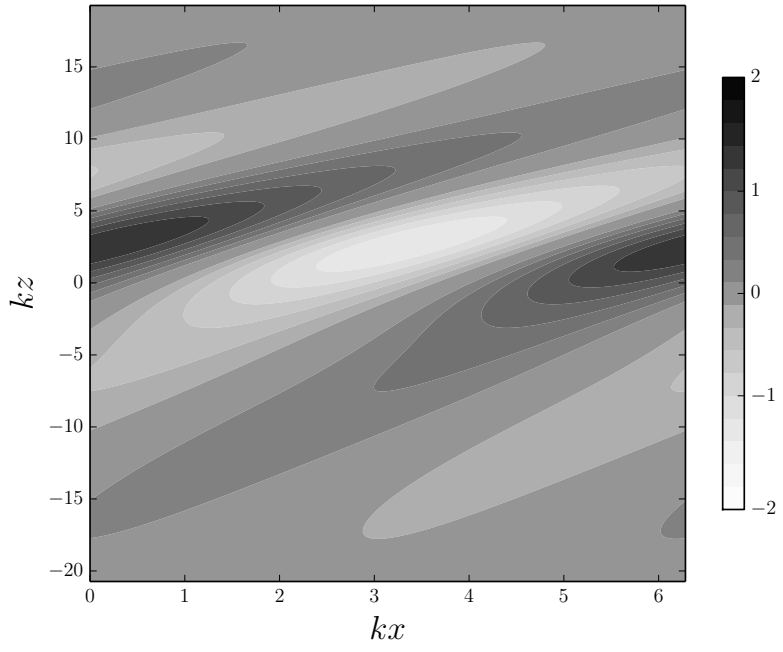

(b) $N_1\tau \approx 0$

Fig. 8: Contours of vertical velocity in a single layer of constant N with $n_1/k = 0.4$, $\epsilon = 0.025$, and $\alpha = 0.1$.

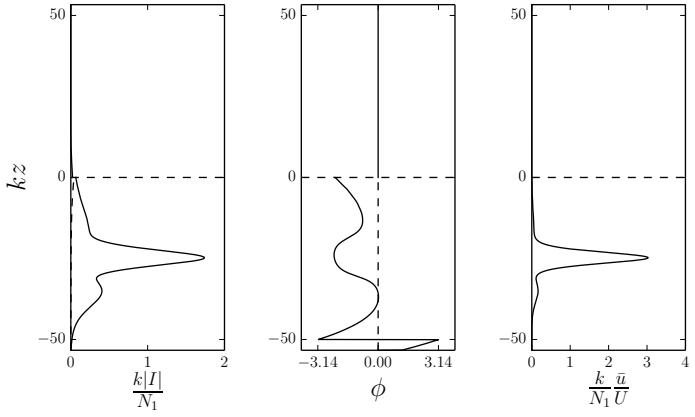

(a) $N_1\tau \approx -80$

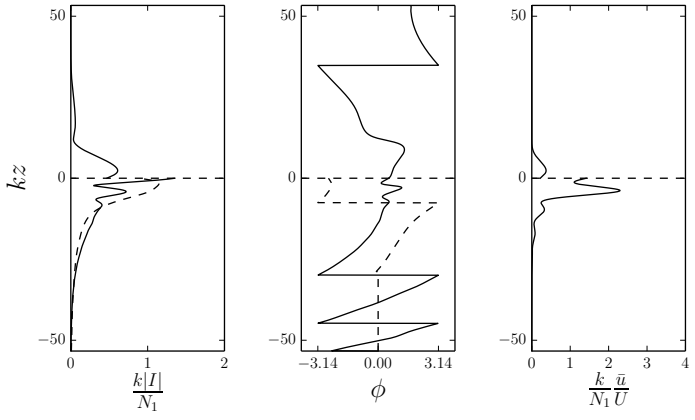

(b) $N_1\tau \approx 0$

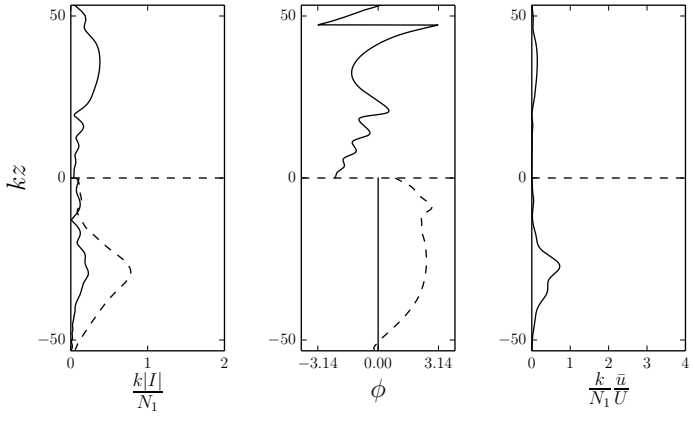

(c) $N_1\tau \approx +80$

Fig. 9: Vertical profiles of the wave magnitude (left panel), phase (center panel), and mean flow (right panel) at three times in two layers. The parameter values are $n_1/k = 0.4$, $N_2/N_1 = 2$, $\epsilon = 0.025$, and $\alpha = 0.1$.

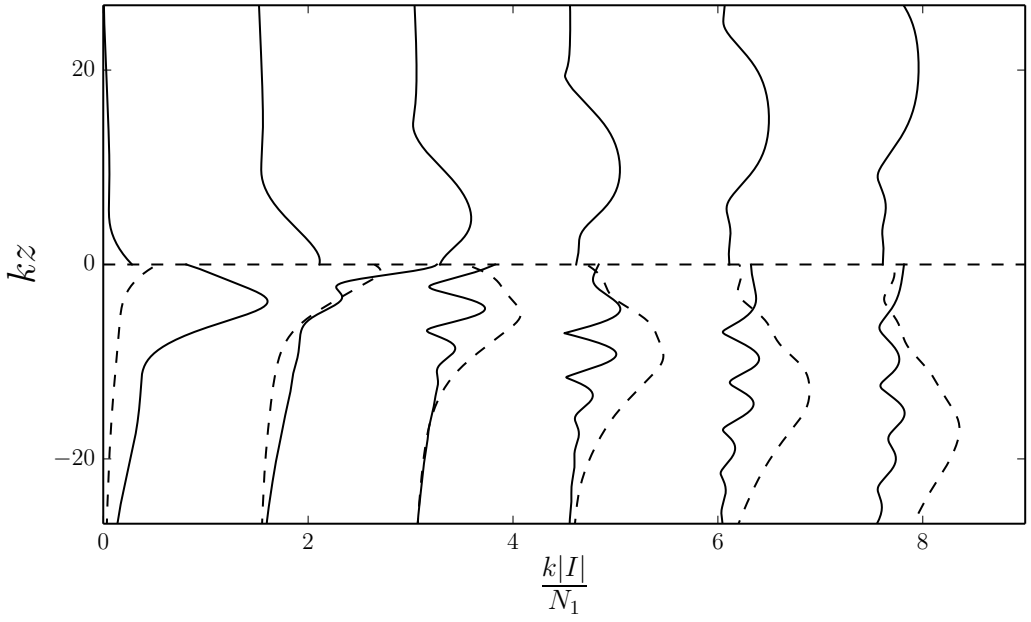

Fig. 10: Vertical profiles of the wave magnitude in two layers for a sequence of times. Each profile is shifted by a value of 1.5 for display. The parameter values are $n_1/k = 0.4$, $N_2/N_1 = 2$, $\epsilon = 0.025$, and $\alpha = 0.1$.

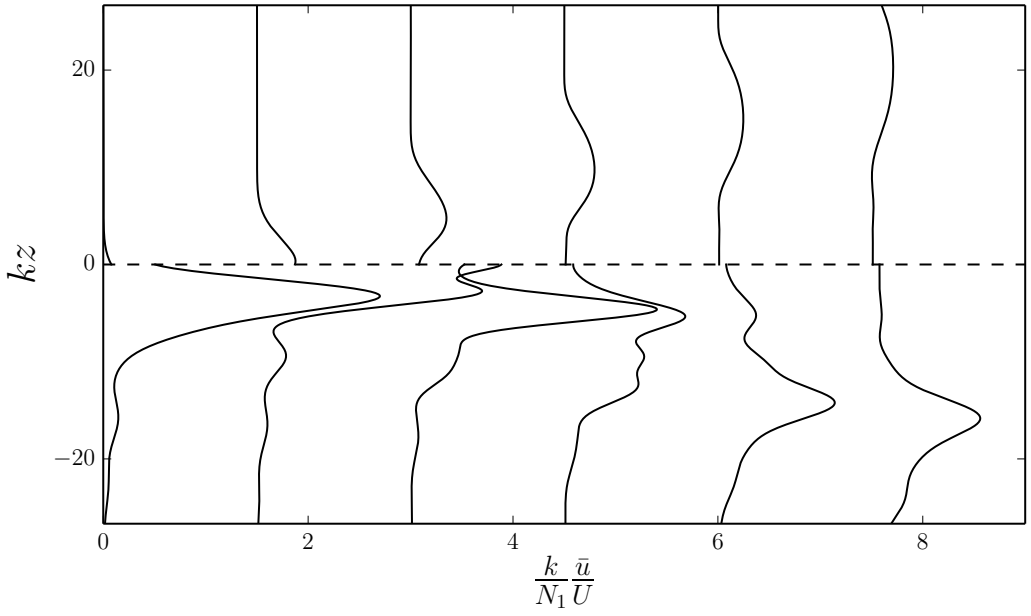

Fig. 11: Vertical profiles of the mean flow in two layers for a sequence of times. Each profile is shifted by a value of 1.5 for display. The parameter values are $n_1/k = 0.4$, $N_2/N_1 = 2$, $\epsilon = 0.025$, and $\alpha = 0.1$.

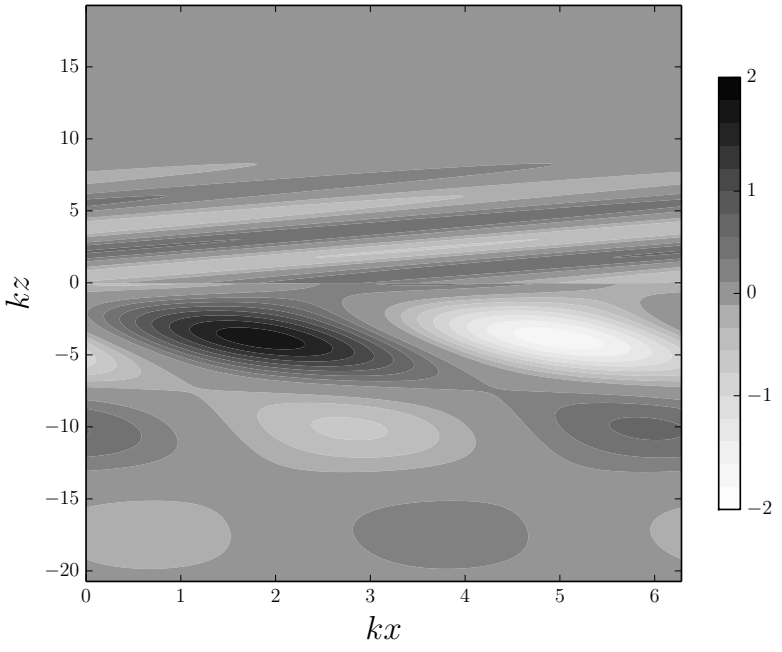

Fig. 12: Contours of vertical velocity at $\tau = \approx 0$ in two layers. The parameter values are $n_1/k = 0.4$, $N_2/N_1 = 2$, $\epsilon = 0.025$, and $\alpha = 0.1$.

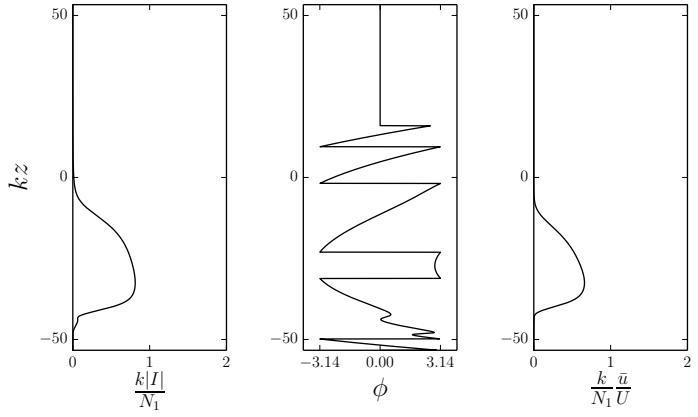

(a) $N_1\tau \approx -77$

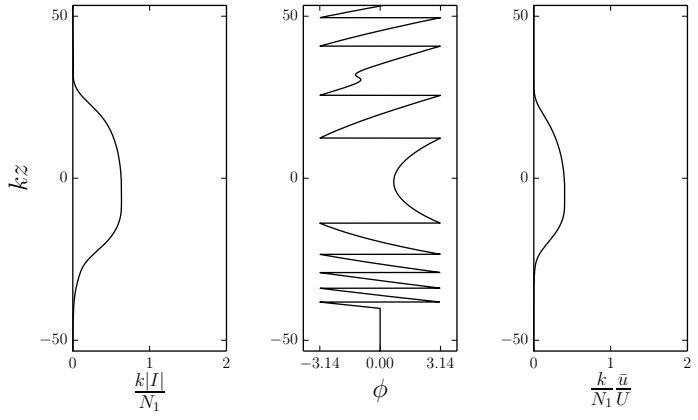

(b) $N_1\tau \approx 0$

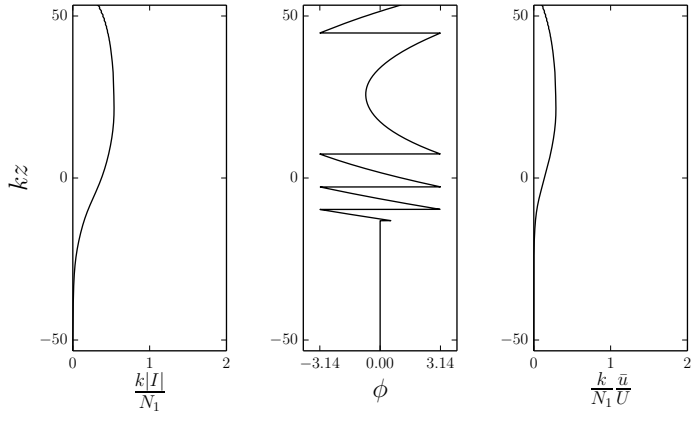

(c) $N_1\tau \approx +77$

Fig. 13: Vertical profiles of the wave magnitude (left panel), phase (center panel), and mean flow (right panel) at three times in a single layer of constant N with $n_1/k = 1$, $\epsilon = 0.025$, and $\alpha = 0.1$.

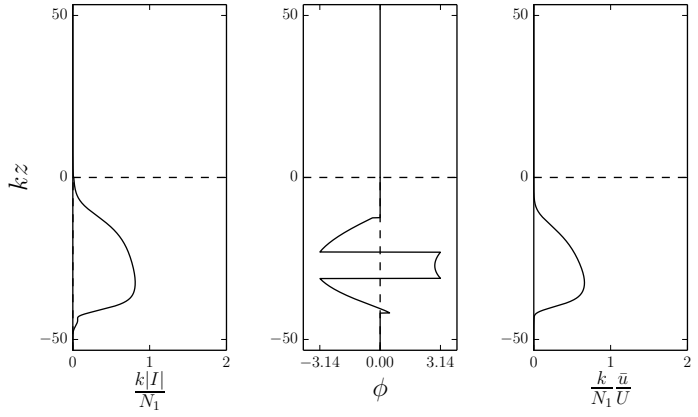

(a) $N_1\tau \approx -77$

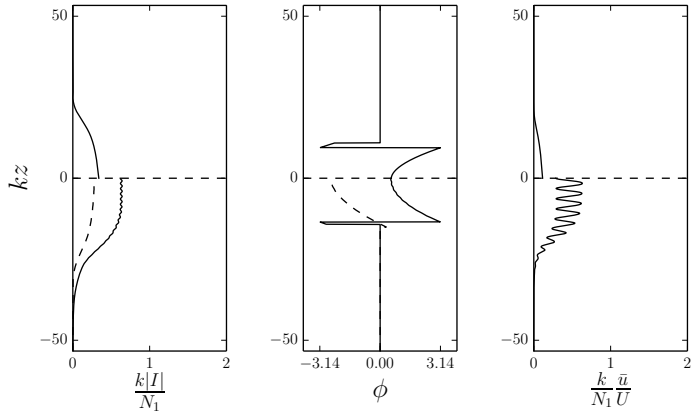

(b) $N_1\tau \approx 0$

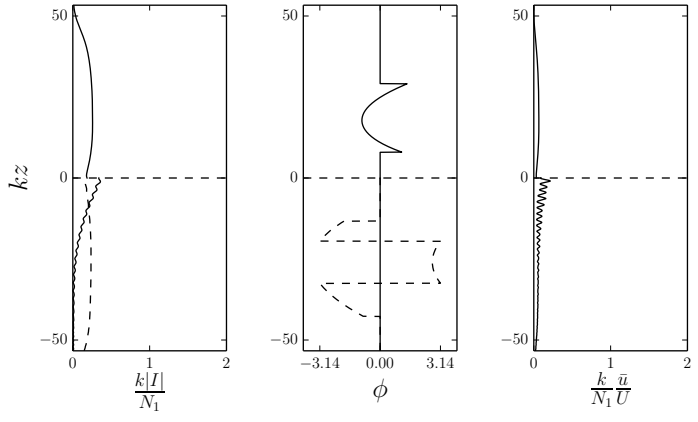

(c) $N_1\tau \approx +77$

Fig. 14: Vertical profiles of the wave magnitude (left panel), phase (center panel), and mean flow (right panel) at three times in two layers. The parameter values are $n_1/k = 1$, $N_2/N_1 = 2$, $\epsilon = 0.025$, and $\alpha = 0.1$.

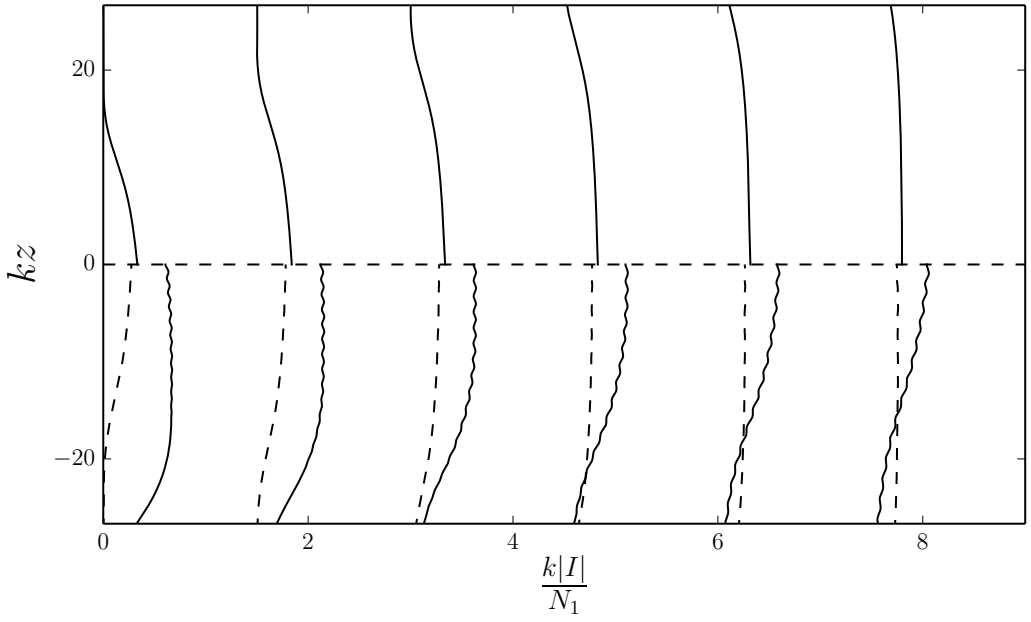

Fig. 15: Vertical profiles of the wave magnitude in two layers for a sequence of times. Each profile is shifted by a value of 1.5 for display. The parameter values are $n_1/k = 1$, $N_2/N_1 = 2$ $\epsilon = 0.025$, and $\alpha = 0.1$.

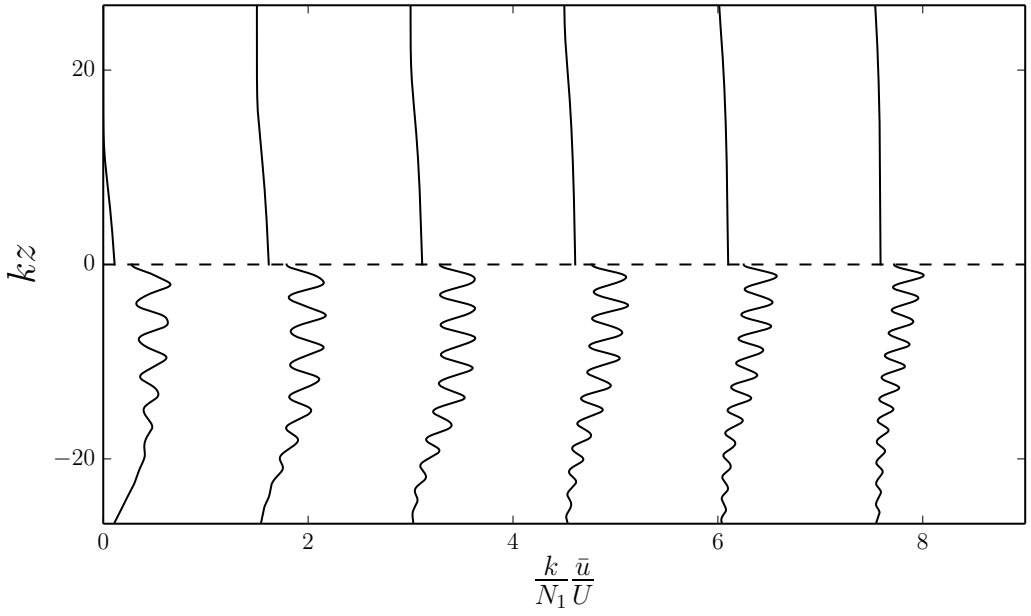

Fig. 16: Vertical profiles of the mean flow in two layers for a sequence of times. Each profile is shifted by a value of 1.5 for display. The parameter values are $n_1/k = 1$, $N_2/N_1 = 2$, $\epsilon = 0.025$, and $\alpha = 0.1$.

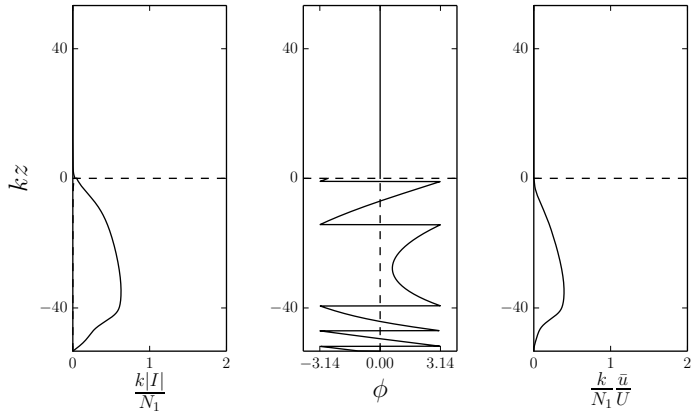

(a) $N_1\tau \approx -98$

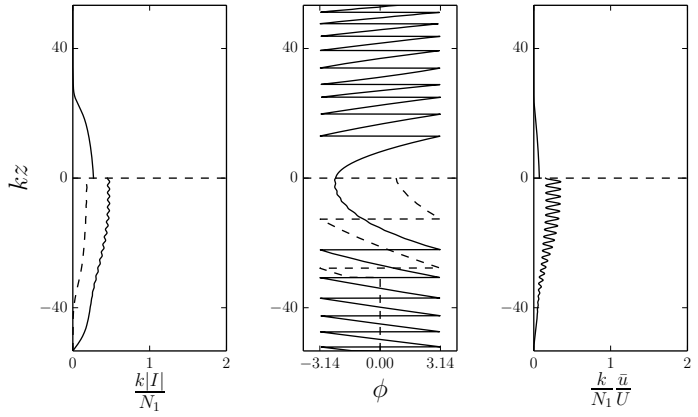

(b) $N_1\tau \approx 0$

Fig. 17: Vertical profiles of the wave magnitude (left panel), phase (center panel), and mean flow (right panel) at three times in two layers. The parameter values are $n_1/k = \sqrt{2}$, $N_2/N_1 = 2$, $\epsilon = 0.025$, and $\alpha = 0.1$.

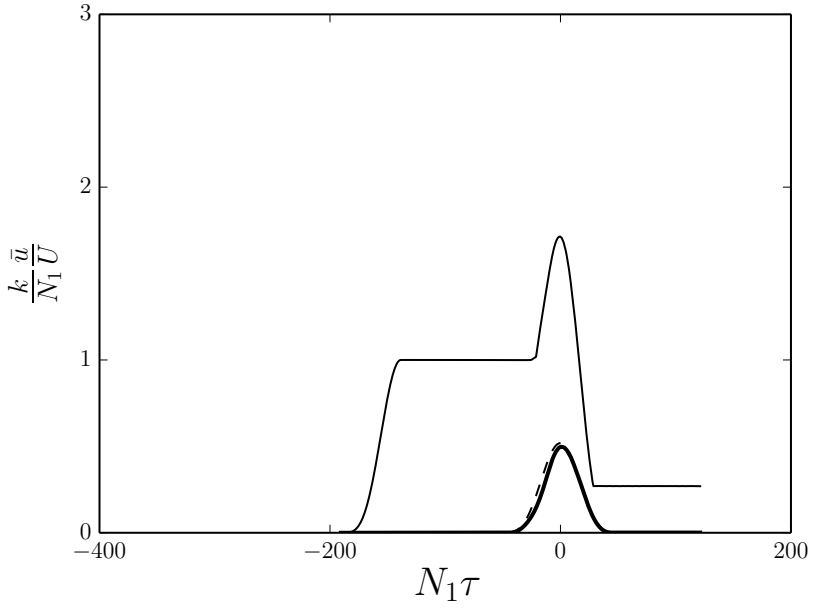

Fig. 18: Time history of the maximum of the mean flow. The dashed line is the velocity jump at the interface while the thick solid line that is the maximum the interference mean $\bar{u}_i$. The parameter values are $n_1/k = 1/\sqrt{2}$, $N_2/N_1 = 2$, $\epsilon = 0.025$, and $\alpha = 0.1$.

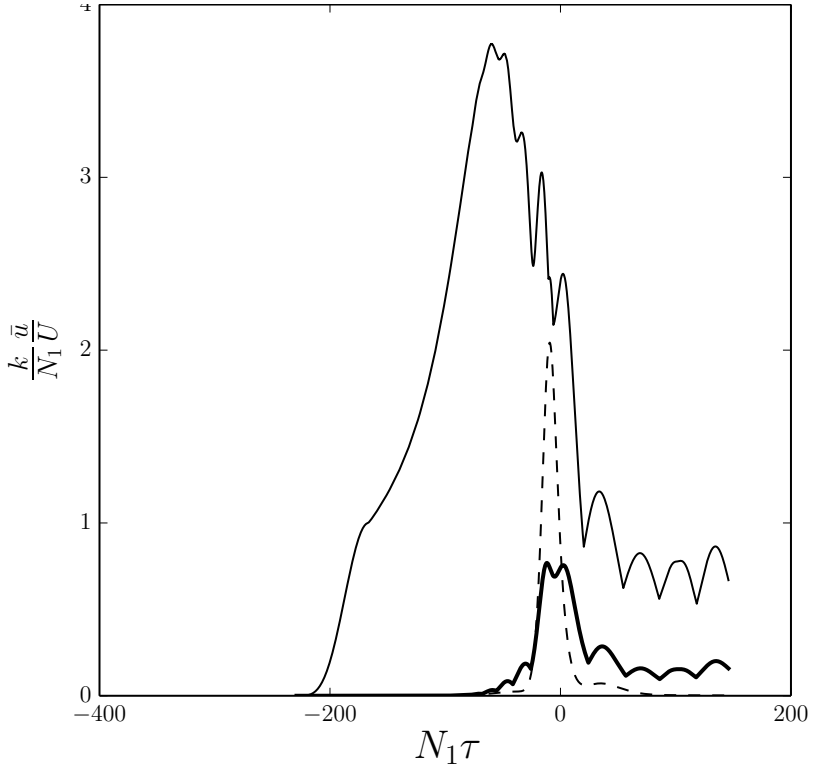

Fig. 19: Time history of the maximum of the mean flow. The dashed line is the velocity jump at the interface while the thick solid line that is the maximum the interference mean $\bar{u}_i$. The parameter values are $n_1/k = 0.4$, $N_2/N_1 = 2$, $\epsilon = 0.025$, and $\alpha = 0.1$.

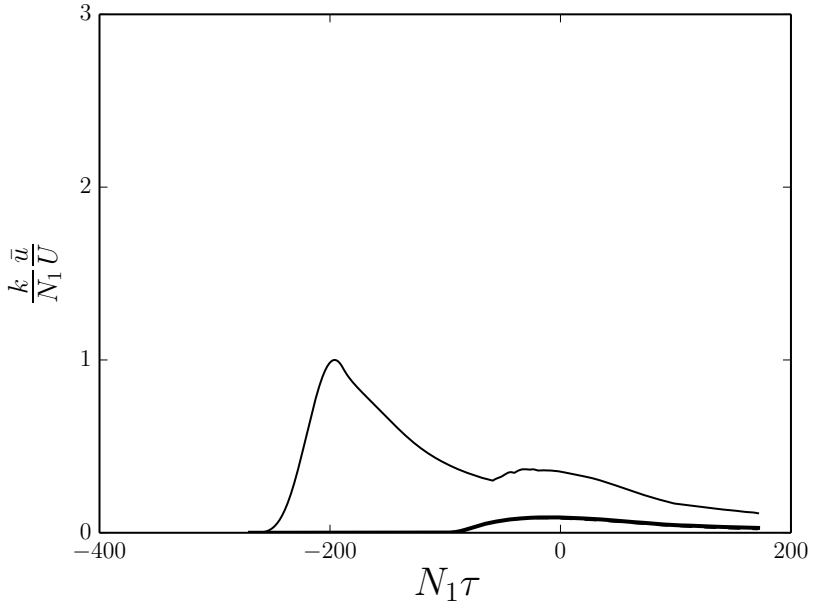

Fig. 20: Time history of the maximum of the mean flow. The dashed line is the velocity jump at the interface while the thick solid line that is the maximum the interference mean $\bar{u}_i$. The parameter values are $n_1/k = \sqrt{2}$, $N_2/N_1 = 2$ $\epsilon = 0.025$, and $\alpha = 0.1$.

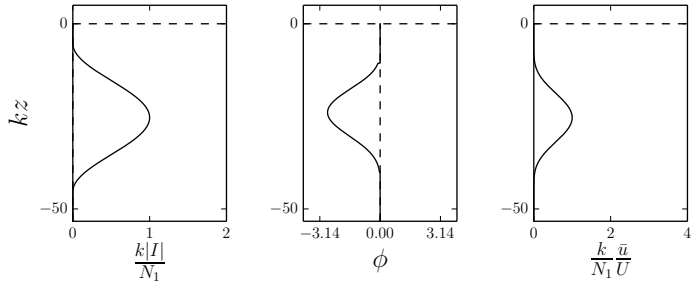

(a) $N_1\tau \approx -65$

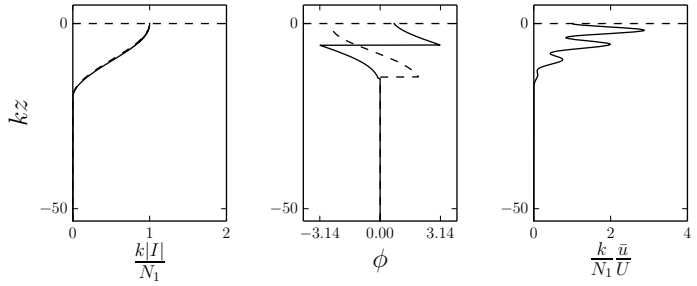

(b) $N_1\tau \approx 0$

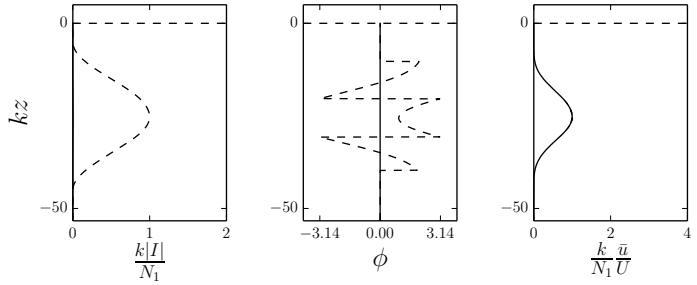

(c) $N_1\tau \approx +65$

Fig. 21: Vertical profiles of the wave magnitude (left panel), phase (center panel), and mean flow (right panel) at three time values with a solid lid, with $n_1/k = 1/\sqrt{2}$, $\epsilon = 0.025$, and $\alpha = 0.1$.